

Genetic Design of Personalized Slag for Manufacturing Die Steel via Electroslag Remelting Method and an Industrial Application Case

Z.H. Jiang¹, Y.M. Li², J.L. Tian³ and J.W. Dong⁴

1. Professor, Northeastern University, Shenyang 110819, China. jiangzh@smm.neu.edu.cn
2. PhD candidate, Northeastern University, Shenyang 110819, China. 15984327096@163.com
3. Associate Professor, Northeastern University, Shenyang 110819, China. neujialong@163.com
4. PhD candidate, Northeastern University, Shenyang 110819, China. neuemta@163.com

Keywords: Electroslag remelting; Slag composition design; Genetic algorithm; Die steel; Inclusions.

ABSTRACT

Electroslag remelting is widely used to produce various special steels, mainly because of its ability to provide high cleanliness and excellent homogeneity of ingot. Undoubtedly an optimal slag plays a key role in removing inclusions and enhancing the mechanical properties of a specific special steel. In order to improve the metallurgical performance of the slag in electroslag refining of die steel, a variety of slags have already been developed using traditional trial-and-error methods. Nonetheless, these slags may not be inherently optimal for the specific requirements of actual die steel refining processes. In this work, we have designed a CaF_2 - CaO - Al_2O_3 - SiO_2 - MgO quinary slag system using genetic algorithms method aiming to remove the existing large size inclusions (D and Ds type) in high quality die steel. The comprehensive effects of five components (CaF_2 , CaO , Al_2O_3 , SiO_2 and MgO) were studied based on existing fundamental theory. The slag composition was screened considering the parameters such as melting point, electrical conductivity, calcium ion concentration, and appropriate viscosity etc. Furthermore, the candidate optimal slag was applied in the industrial production of die steel by electroslag remelting method. The detection results indicate that majority large inclusions (D and Ds type) have been successfully removed, showing significant advantage to traditional slags. This result has demonstrated the genetic method to be efficient and reliable. In addition, depending on the personalized demand of other steel and alloys, this method allows for the adjustment of the screening frameworks and processes to develop the candidate optimal slags. This method has not been reported previously in the field of electroslag composition design, and compared with the traditional trial-and-error method, the new method will save a lot of time and experimental costs.

1. INTRODUCTION

In steel production, the presence of nonmetallic inclusions often results in the formation of micropores and cracks, initiating fatigue fracture and structural defects (Sabih, Wanjara and Nemes, 2005). To counteract this, the electroslag remelting (ESR) process is employed to achieve a uniform composition, structural densification, and the removal of inclusions, thereby increasing steel purity and quality (Jiang, Dong, Geng et al, 2023). In the ESR process, the role of slag is critically important, acting as a decisive factor in determining the quality of electroslag ingots (Sebastian and Bernd, 2015; Shi, Li, Cho et al, 2015; Shi, 2020). Consequently, precise design and control of the slag composition are essential.

Traditionally, the design of slag composition relies on an empirical trial-and-error approach. While practical, this method can be time-consuming and may not yield optimal results, necessitating a more systematic and scientifically grounded strategy (Dong, Jang and Yu, 2016; Dong, Jiang, Cao et al, 2014). In response to the diverse metallurgical requirements in the ESR process, modern slags have transcended traditional constituents such as CaF_2 and Al_2O_3 (Schneider, Molnar, Kloesch et al, 2019; Sebastian and Bernd, 2015) and specific quantities of CaO , MgO , and SiO_2 have been incorporated. The concentrations of slag components could vary widely to meet the specific requirements of different steel categories (Sebastian and Bernd 2015; Duan, 2020; Ju, Ji, Tang et

al, 2020). The typical composition of $\text{CaF}_2\text{-CaO-Al}_2\text{O}_3$ -based ESR slag includes 40%–70% CaF_2 , 0%–40% CaO , and 20%–40% Al_2O_3 , with small amounts of SiO_2 and MgO (Ju, Gu and Zhang, 2021, Wan, Shi, Yu et al, 2022).

In material design field, genetic algorithms have been extensively utilized (Campbell and Olson, 2000; Xu, del Castillo and van der Zwaag, 2009). This study pioneers genetic algorithms for optimizing slag composition, a previously unexplored technique in slag composition design. Both considering the ESR ingots' metallurgical quality and surface quality, the slag's physical and chemical characteristics including melting point, viscosity, electrical conductivity, basicity, density, and ion/molecule concentrations have been identified as the slag system's crucial parameters ("genes"), leveraging genetic algorithms to select superior slag compositions.

In the conventional trial-and-error approach, optimizing slag compositions is restricted to minor adjustments, typically limited to a few percentage points from the original composition. This method limits the number of experiments and frequently yields suboptimal outcomes. However, the application of genetic algorithms allows for a significantly broader range of variation for each component in the slag based on years of production experience. This approach, generating an extensive dataset, considerably enhances the likelihood of identifying the optimal composition window in the new generation of slag compositions. Moreover, this approach can save time and material costs compared to conventional trial-and-error methods.

This novel slag design approach has been applied in the die steel production. When using traditional ANF-6 slag, excessive D and Ds inclusions in 1.2343 die steel were usually detected. The D and Ds inclusions are mainly composed of $\text{CaO-Al}_2\text{O}_3$ or $\text{CaO-MgO-Al}_2\text{O}_3$. These inclusions are challenging to remove during electroslag remelting and lead to minute point-like formations in ingots (Guo, Xia, Shen et al, 2021), detrimentally affecting the steel's plasticity, toughness, fatigue resistance, workability, and specific physical properties (Ragnarsson and Sichen, 2009). This work employs genetic algorithms for slag design, successfully developing a new slag used for manufacturing high cleanliness 1.2343 die steel. The newly developed slag preserves the surface quality of the ESR ingot and effectively mitigates the issue of excessive D and Ds inclusions.

2. METHODS

First, we created a comprehensive database incorporating all possible combinations of slag compositions. This study identified six physicochemical properties—density, melting point, electrical conductivity, optical basicity, viscosity, and ion/molecule concentration—as key parameters ("genes") of the slag system. Subsequently, genetic algorithms are utilized to determine slag compositions exhibiting superior performance. For instance, the calcium ion "gene" activity is adjusted to mitigate excessive D and Ds inclusions in 1.2343 die steel. Figure 1 shows the process of the genetic algorithm employed to screen the slag composition.

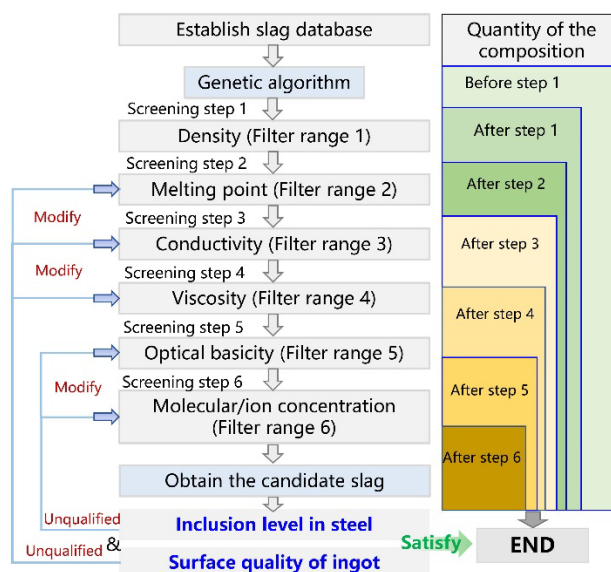


FIG 1 – Genetic algorithm employed in the selection of slag composition

2.1 Establishment of slag composition combinations

Relying on extensive theoretical and practical experience, this study sets specific variation ranges for every component in the quinary slag system, as detailed in Table 1, to streamline calculations (Ju, Gu and Zhang, 2021; Duan, 2020; Wan, Shi, Yu et al, 2022; Dong, 2007). Employing a 1% step increment for component variation, Python programming generated a total of 138,347 unique combinations.

TABLE 1 – Concentration ranges for all components utilized in the optimization (in weight fraction)

	CaO	SiO ₂	Al ₂ O ₃	MgO	CaF ₂
Min	0	0	20	0	30
Max	40	15	40	15	70

2.2 Prediction of physical parameters of slag

2.2.1 Prediction of density of slag

The density of various slag compositions could be obtained based on the following empirical formula (Jiang, Dong, Geng et al, 2015):

$$\frac{100}{\rho} = 0.416m(\text{SiO}_2) + 0.303m(\text{CaO}) + 0.372m(\text{MgO}) + 0.328m(\text{Al}_2\text{O}_3) + 0.389m(\text{CaF}_2) \quad (1)$$

where m(i) represents the mass of substance i in 100 g of slag, expressed in grams, and the unit for density is grams per cubic centimeter (g/cm³).

2.2.2 Prediction of melting point of slag

To calculate the melting point of various slags, the computational model has been proposed in previous work (Zhao, Zhang and Ju, 2013):

$$\begin{aligned} T = & 1682.9399 + 164.479X_1 - 162.6886X_2 + 250.209X_3 - 1415.624X_4 \\ & - 819.2188X_5 - 7937.5X_1X_2 + 8687.5X_1X_3 - 8262.5X_1X_4 \\ & + 146.875X_1X_5 - 12725X_2X_3 + 5075X_2X_4 + 1068.75X_2X_5 \\ & - 1575X_3X_4 + 181.25X_3X_5 + 3906.25X_4X_5 + 1751.042X_1^2 \\ & + 15.88542X_2^2 - 5495.84X_3^2 + 504.1668X_4^2 + 244.0104X_5^2 \end{aligned} \quad (2)$$

where X₁ is the mass percent of Al₂O₃, X₂ is the mass percent of MgO, X₃ is the mass percent of SiO₂, X₄ is the mass percent of CaO, X₅ is the mass percent of CaF₂, and T represents the temperature in degrees Celsius.

2.2.3 Prediction of conductivity of slag

The relationship between conductivity and slag composition could be quantified by the following formula (Ju, Lv and Jiao, 2012).

$$K(\Omega^{-1}\cdot\text{cm}^{-1}) = 100\exp(1.911 - 1.38x_x - 5.69x_x^2) + 0.39(T - 1973) \quad (3)$$

$$x_x = x(\text{Al}_2\text{O}_3) + 0.2x(\text{CaO}) + 0.8x(\text{MgO}) + 0.75x(\text{SiO}_2) + 0.2x(\text{CaF}_2) \quad (4)$$

where X (i) represents the molar percentage of component i.

2.2.4 Prediction of optical basicity of slag

The optical basicity of slag containing calcium fluoride could be calculated using the following formula (Zhang, Chou and Pal, 2013):

$$\Lambda = \sum \Lambda_i \times X_i \quad (5)$$

$$X_i = \frac{A_i \times n_i \times N_i}{\sum \left[\frac{A_i \times n_i \times N_i}{2} \right]} \quad (6)$$

where A_i denotes the anionic charge of component i , n_i is the anionic number of component i , N_i denotes the mole fraction of component i , and Λ_i denotes the optical basicity of component i . The optical basicities of each constituent element are specified in Table 2, offering comprehensive quantitative data (Zhang, Chou and Pal, 2013; Hao and Wang, 2016).

TABLE 2 – Optical basicity value for each component

Component	Optical basicity
CaO	1
MgO	0.92
Al ₂ O ₃	0.66
SiO ₂	0.47
CaF ₂	0.67

2.2.5 Prediction of molecule and ion activity in the slag

To determine the activity of molecule and ions in CaF₂-Al₂O₃-CaO-SiO₂-MgO slag, this work employs the molecule ion coexistence theory (MICT), examining ternary phase diagrams such as CaO-CaF₂-SiO₂, CaO-CaF₂-MgO, CaO-CaF₂-Al₂O₃, CaO-SiO₂-MgO, CaO-SiO₂-Al₂O₃, CaO-MgO-Al₂O₃, CaF₂-SiO₂-MgO, CaF₂-SiO₂-Al₂O₃, CaF₂-MgO-Al₂O₃, and SiO₂-MgO-Al₂O₃ (Guillot and Guissani, 1996; Sun, Yang, Zhang et al, 2021; Zhao, Li and He, 2022; Duan, 2020; Dong, 2007). Finally, the structural units in CaO-CaF₂-SiO₂-MgO-Al₂O₃ slag system are identified as four simple ions (Ca²⁺, Mg²⁺, O²⁻, F⁻), two simple molecules (Al₂O₃, SiO₂), along with 23 complex molecules. Using thermodynamic data provided in Table 3 and Python programming, the concentration of molecule and ions in the molten slags could be calculated.

TABLE 3 – Chemical reaction formulas of complex molecules that may be formed, their standard Gibbs free energy changes, and mass action concentrations of structural units in the CaF₂-Al₂O₃-CaO-SiO₂-MgO system

Reactions	ΔG_f° (J/mol)	Mass action concentration
$\text{Ca}^{2+} + \text{O}^{2-} = \text{CaO}$	/	$N_1 = N_{\text{Ca}^{2+}} + N_{\text{O}^{2-}} = \frac{2x_1}{\sum X}$
$\text{Mg}^{2+} + \text{O}^{2-} = \text{MgO}$	/	$N_2 = N_{\text{Mg}^{2+}} + N_{\text{O}^{2-}} = \frac{2x_1}{\sum X}$
$\text{Ca}^{2+} + 2\text{F}^- = \text{CaF}_2$	/	$N_3 = N_{\text{Ca}^{2+}} + 2N_{\text{F}^-} = \frac{3x_1}{\sum X}$
SiO ₂	/	$N_4 = \frac{x_4}{\sum X}$
MgO	/	$N_5 = \frac{x_5}{\sum X}$
$3(\text{Ca}^{2+} + \text{O}^{2-}) + \text{Al}_2\text{O}_3 = (3\text{CaO} \cdot \text{Al}_2\text{O}_3)$	$\Delta G_1^\circ = -21757 - 29.288T$	$N_6 = K_1 N_1^3 N_5$
$12(\text{Ca}^{2+} + \text{O}^{2-}) + 7\text{Al}_2\text{O}_3 = (12\text{CaO} \cdot 7\text{Al}_2\text{O}_3)$	$\Delta G_2^\circ = 617977 - 612.119T$	$N_7 = K_2 N_1^{12} N_5^7$

$(\text{Ca}^{2+} + \text{O}^{2-}) + \text{Al}_2\text{O}_3 = (\text{CaO} \cdot \text{Al}_2\text{O}_3)$	$\Delta G_3^0 = 59413 - 59.4137T$	$N_8 = K_3 N_1 N_5$
$(\text{Ca}^{2+} + \text{O}^{2-}) + 2\text{Al}_2\text{O}_3 = (\text{CaO} \cdot 2\text{Al}_2\text{O}_3)$	$\Delta G_4^0 = -16736 - 25.522T$	$N_9 = K_4 N_1 N_5^2$
$(\text{Ca}^{2+} + \text{O}^{2-}) + 6\text{Al}_2\text{O}_3 = (\text{CaO} \cdot 6\text{Al}_2\text{O}_3)$	$\Delta G_5^0 = -22594 - 31.798T$	$N_{10} = K_5 N_1 N_5^6$
$(\text{Mg}^{2+} + \text{O}^{2-}) + \text{Al}_2\text{O}_3 = (\text{MgO} \cdot \text{Al}_2\text{O}_3)$	$\Delta G_6^0 = -18828 - 6.276T$	$N_{11} = K_6 N_2 N_5$
$3(\text{Ca}^{2+} + \text{O}^{2-}) + 2\text{Al}_2\text{O}_3 + (\text{Ca}^{2+} + 2\text{F}^-)$ $= (3\text{CaO} \cdot 2\text{Al}_2\text{O}_3 \cdot \text{CaF}_2)$	$\Delta G_7^0 = -44492 - 73.15T$	$N_{12} = K_7 N_1^3 N_5^2 N_3$
$11(\text{Ca}^{2+} + \text{O}^{2-}) + 7\text{Al}_2\text{O}_3 + (\text{Ca}^{2+} + 2\text{F}^-)$ $= (11\text{CaO} \cdot 7\text{Al}_2\text{O}_3 \cdot \text{CaF}_2)$	$\Delta G_8^0 = -228760 - 155.8T$	$N_{13} = K_8 N_1^{11} N_5^7 N_3$
$3(\text{Ca}^{2+} + \text{O}^{2-}) + \text{SiO}_2 = (3\text{CaO} \cdot \text{SiO}_2)$	$\Delta G_9^0 = -118826 - 6.694T$	$N_{14} = K_9 N_1^3 N_4$
$3(\text{Ca}^{2+} + \text{O}^{2-}) + 2\text{SiO}_2 = (3\text{CaO} \cdot 2\text{SiO}_2)$	$\Delta G_{10}^0 = -236814 + 9.623T$	$N_{15} = K_{10} N_1^3 N_4^2$
$2(\text{Ca}^{2+} + \text{O}^{2-}) + \text{SiO}_2 = (2\text{CaO} \cdot \text{SiO}_2)$	$\Delta G_{11}^0 = -102090 - 24.26T$	$N_{16} = K_{11} N_1^2 N_4$
$(\text{Ca}^{2+} + \text{O}^{2-}) + \text{SiO}_2 = (\text{CaO} \cdot \text{SiO}_2)$	$\Delta G_{12}^0 = -21757 - 36.819T$	$N_{17} = K_{12} N_1 N_4$
$2(\text{Mg}^{2+} + \text{O}^{2-}) + (\text{SiO}_2) = (2\text{MgO} \cdot \text{SiO}_2)$	$\Delta G_{13}^0 = -56902 - 3.347T$	$N_{18} = K_{13} N_2^2 N_4$
$(\text{Mg}^{2+} + \text{O}^{2-}) + (\text{SiO}_2) = (\text{MgO} \cdot \text{SiO}_2)$	$\Delta G_{14}^0 = -23849 - 29.706T$	$N_{19} = K_{14} N_2 N_4$
$3\text{Al}_2\text{O}_3 + 2\text{SiO}_2 = (3\text{Al}_2\text{O}_3 \cdot 2\text{SiO}_2)$	$\Delta G_{15}^0 = -4354 - 10.467T$	$N_{20} = K_{15} N_5^3 N_4^2$
$2(\text{Ca}^{2+} + \text{O}^{2-}) + \text{Al}_2\text{O}_3 + \text{SiO}_2$ $= (2\text{CaO} \cdot \text{Al}_2\text{O}_3 \cdot \text{SiO}_2)$	$\Delta G_{16}^0 = -116315 - 38.911T$	$N_{21} = K_{16} N_1^2 N_5 N_4$
$(\text{Ca}^{2+} + \text{O}^{2-}) + \text{Al}_2\text{O}_3 + 2\text{SiO}_2$ $= (\text{CaO} \cdot \text{Al}_2\text{O}_3 \cdot 2\text{SiO}_2)$	$\Delta G_{17}^0 = -4184 - 73.638T$	$N_{22} = K_{17} N_1 N_5 N_4^2$
$(\text{Ca}^{2+} + \text{O}^{2-}) + (\text{Mg}^{2+} + \text{O}^{2-}) + \text{SiO}_2$ $= (\text{CaO} \cdot \text{MgO} \cdot \text{SiO}_2)$	$\Delta G_{18}^0 = -124683 + 3.766T$	$N_{23} = K_{18} N_1 N_2 N_4$
$(\text{Ca}^{2+} + \text{O}^{2-}) + (\text{Mg}^{2+} + \text{O}^{2-}) + 2\text{SiO}_2$ $= (\text{CaO} \cdot \text{MgO} \cdot 2\text{SiO}_2)$	$\Delta G_{19}^0 = -80333 + 51.882T$	$N_{24} = K_{19} N_1 N_2 N_4^2$
$2(\text{Ca}^{2+} + \text{O}^{2-}) + (\text{Mg}^{2+} + \text{O}^{2-}) + 2\text{SiO}_2$ $= (2\text{CaO} \cdot \text{MgO} \cdot 2\text{SiO}_2)$	$\Delta G_{20}^0 = -73638 + 63.597T$	$N_{25} = K_{20} N_1^2 N_2 N_4^2$
$3(\text{Ca}^{2+} + \text{O}^{2-}) + (\text{Mg}^{2+} + \text{O}^{2-}) + 2\text{SiO}_2$ $= (3\text{CaO} \cdot \text{MgO} \cdot 2\text{SiO}_2)$	$\Delta G_{21}^0 = -205016 - 31.798T$	$N_{26} = K_{21} N_1^3 N_2 N_4^2$
$2(\text{Mg}^{2+} + \text{O}^{2-}) + 2\text{Al}_2\text{O}_3 + 5\text{SiO}_2$ $= (2\text{MgO} \cdot 2\text{Al}_2\text{O}_3 \cdot 5\text{SiO}_2)$	$\Delta G_{22}^0 = -14422 - 14.808T$	$N_{27} = K_{21} N_2^2 N_5^2 N_4^5$
$3(\text{Ca}^{2+} + \text{O}^{2-}) + 2\text{SiO}_2 + (\text{Ca}^{2+} + 2\text{F}^-)$ $= (3\text{CaO} \cdot 2\text{SiO}_2 \cdot \text{CaF}_2)$	$\Delta G_{23}^0 = -255180 - 8.20T$	$N_{28} = K_{22} N_1^3 N_4^2 N_3$

2.2.6 Prediction of viscosity of slag

This work determined the viscosity of slag at 1550°C using Factsage 8.2, incorporating variations in slag components such as CaF₂ (30%–70%), Al₂O₃ (20%–40%), CaO (0%–40%), MgO (0%–15%), and SiO₂ (0%–15%) with 2% step increments. This approach reduced the potential combinations to 9,717, decreasing computational requirements. A quadratic polynomial fitting analysis of these combinations, executed using Python, demonstrated high accuracy with an average absolute error of 1.7708%, thereby validating its applicability to the larger dataset of 138,347 combinations. The viscosity fitting results at 1550°C are as follows:

$$\begin{aligned} \eta = & 43342344120.47134 + 2260652.27797391 \cdot A \\ & - 492659.33981768 \cdot B - 247519.83942283 \cdot C \\ & - 442894.24850764 \cdot D - 465902.84576523 \cdot E \\ & - 4356840.93482216 \cdot A^2 - 8686148.7534862 \cdot A \cdot B \\ & - 8688600.14848205 \cdot A \cdot C - 8686646.40438652 \cdot A \cdot D \\ & - 8686416.31844023 \cdot A \cdot E - 4329307.81862237 \cdot B^2 \\ & - 8661067.03228913 \cdot B \cdot C - 8659113.28819614 \cdot B \cdot D \\ & - 8658883.20218896 \cdot B \cdot E - 4331759.21364703 \cdot C^2 \\ & - 8661564.683198 \cdot C \cdot D - 8661334.59722407 \cdot C \cdot E \\ & - 4329805.46955192 \cdot D^2 - 8659380.8531375 \cdot D \cdot E \\ & - 4329575.38355188 \cdot E^2 \end{aligned} \quad (7)$$

where A, B, C, D, and E denote the mass percentages of CaF₂, Al₂O₃, CaO, MgO, and SiO₂, respectively, while η represents the slag system's viscosity at 1550°C, measured in Pa·s.

2.3 Screening method

The ESR product in this work is 1.2343 die steel and the chemical composition of this steel is presented in Table 4. Initially the 1.2343 die steel was remelted with ANF-6 slag, primarily composed of 70% CaF₂ and 30% Al₂O₃. Thus this work focused on optimizing the slag composition based on ANF-6 slag.

TABLE 4 – Chemical composition of 1.2343 die steel

Element	C	Mn	Si	Cr	Mo	P	S
wt%	0.38–0.45	0.30–0.50	0.9–1.0	4.8–5.5	1.2–1.5	0.03 max	0.03 max

The initial step involves calculating various physical properties of the original slag (ANF-6 slag with 70%CaF₂ and 30%Al₂O₃), with values presented in Table 5. Upon calculating the physical property parameters of the original slag, we have chosen it as the reference slag system.

TABLE 5 – Physical parameters of ANF-6 slag

Physical parameters	Numerical value
Densities (g/cm ³)	2.7
Melting point (°C)	1466.8
Conductivity (Ω ⁻¹ ·cm ⁻¹)	2.0
Optical basicity	0.67
Calcium ion activity (mol/g)	0.0067
Viscosity (Pa·s)	0.027

During the process of ESR, metal droplets melting from the consumable electrode tip are subject to the buoyant forces of the slag, which can be quantitatively described by the buoyancy formula $F_{buoyancy} = \rho_{slag} \cdot V_{metal\ drop}$, where $F_{buoyancy}$ represents the buoyant force, ρ_{slag} denotes the density of the slag, and $V_{metal\ drop}$ is the volume of the metal (Duchesne and Hughes, 2017). **The buoyancy force** prolongs the slag-metal reaction time, significantly influencing the metal's purification and alloy composition, and impacts the final product's chemical and microstructural qualities. Thus, the objective is to select a slag composition with a higher density than the ANF-6 slag or the average of all combinations.

Regarding melting point, it is commonly accepted that the slag's melting point should be 100°C–200°C lower than the metal's melting point (Dong, 2007; Jang, Tian, Bo et al, 2023).

In terms of electrical conductivity, optimal conductivity is crucial for electroslag remelting efficiency and ingot quality. Lower conductivity decreases the electrode gap, increasing heat generation. However, lower conductivity may result in short-circuiting and unstable melting. Conversely, high conductivity enlarges the electrode gap, lowering the temperature and increasing heat loss, potentially causing an open arc (Biol, Polat and Saridede, 2015; Liu, Zhang, Wu et al, 2016). Therefore, the slag's conductivity should be slightly lower than that of the ANF-6 slag or just below the median of all slag compositions to achieve a balance between efficiency, stability, and quality.

Concerning optical basicity, higher basicity slags, with elevated CaO content, enhance dephosphorization and desulfurization but may increase gas content in steel; On the contrary, acidic slags are less effective in desulfurization and facilitate gas content reduction, primarily hydrogen. Under protective or vacuum conditions, the advantages of acidic slag diminish (Biol, Polat and Saridede, 2015; Zhang, Chou and Pal, 2013; Hao and Wang, 2016; Dong, 2007). Thus, higher basicity slags are preferable, and the goal is to select a slag composition with optical basicity surpassing that of ANF-6 slag or exceeding the average of all slag combinations, ensuring that the selected basicity is the highest among these values.

Regarding inclusions in 1.2343 die steel, reducing the concentration of free calcium ions in the molten slag is crucial to addressing the excessive D and Ds inclusions. The aim is to lower calcium ion activity in the slag. The objective is to select slag compositions with calcium ion activity lower than that in ANF-6 slag and the average across all slag combinations.

In terms of viscosity, the slag needs to maintain an appropriate viscosity with minimal fluctuation under temperature changes. Optimal viscosity ensures good slag fluidity and is crucial for maintaining the surface quality of the ESR ingots (Sebastian, Johannes and Bernd, 2012). Generally, a lower viscosity is preferred (Dong, 2007; Li and Zhang, 2000). Therefore, the objective is to select slag compositions with a viscosity close to that of the ANF-6 slag or within the median viscosity value of all slag combinations.

2.4 Screening results of the new slag

Based on our analysis and calculations, the criteria for selecting slag compositions are as follows: density of 2.80–2.97 g/cm³, melting point of 1150–1350°C, electrical conductivity of 1–2 Ω⁻¹·cm⁻¹, optical basicity of 0.70–0.82, free calcium ion concentration of 0.0035–0.0067 mol/g, and viscosity of 0.030–0.050 Pa·s.

In Figure 2, the sections highlighted with light blue shading represent the retained results after screening for each physicochemical parameter. After the screening, from the original 138,347 combinations, only 3,961 remain, reducing the dataset to 2.86% of its initial data volume. The average, median, and model values for the filtered residue series are presented in Table 6.

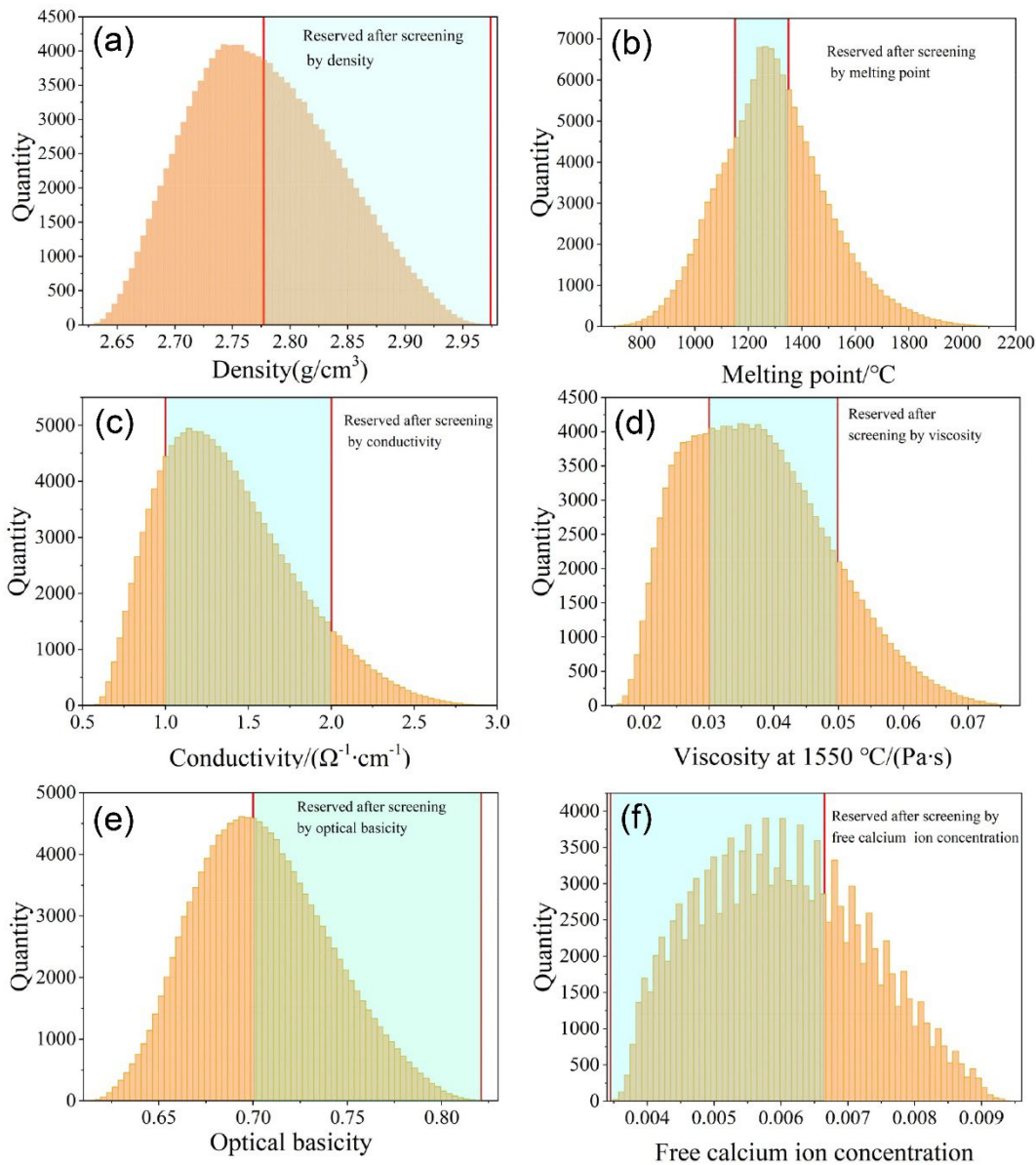


FIG 2 – Screening for each physical property parameter

TABLE 6 – The average, median, and model values for the filtered slag composition

	CaF₂	Al₂O₃	CaO	MgO	SiO₂
Mean value/wt%	43.4	31.8	15.9	4.4	4.5
Median/wt%	43	32	15	4	4
Model/wt%	43	33	15	4	3

Despite narrowing down the viable slag combinations to 2.86% of the original after screening, a wide range of options remains. Considering the limited experimental capacity, it's critical to choose a representative slag composition. To avoid extreme results and ensure experimental reliability, this study calculated the average content of each component, rounding to the nearest whole number for the target slag composition. This method balances the diverse slag characteristics, accurately representing average slag behavior.

Based on the results presented in Table 6, the mass fraction composition of the slag system can be specified as follows: 43% CaF₂, 32% Al₂O₃, 16% CaO, 4% MgO, and 5% SiO₂. This particular slag composition is denoted as the model slag.

3. INDUSTRIAL EXPERIMENTAL VALIDATION

3.1 Industrial experimental procedure

For slag used for industrial trial, it's essential to pre-melt the slag with specified granularity: $\geq 80\%$ of particles between 1-8mm, and $\leq 10\%$ each for particles smaller than 1mm or larger than 8mm. The nominal compositions of the original (ANF-6 Slag) and experimental (Model slag) slags are outlined in Table 7.

Four ESR industrial experiments were performed at a steel plant in China using two different slags: ANF-6 slag and Model slag. Two ESR ingots have been remelted for each slag in a 5000-kg capacity furnace, and the chemical composition of the steel was show in Table 4. The electrodes were melted in an electric arc furnace. After tapping of the melt, the ladle was transferred to a ladle furnace station to reach objective chemical composition and oxygen level. Thereafter, the ladle was sent to the vacuum degassing station to obtain the desired levels of sulphur and hydrogen contents in the melt. At casting station, the electrodes with 2600 mm in length and 550 mm in diameter have been cast using uphill casting technique. Before the experiments, the iron oxide scale was mechanically removed from the electrode surface. Approximately 150 kg of a slag mixture (CaF_2 , Al_2O_3 , CaO , SiO_2 , and MgO) was prepared and introduced into the ESR furnace, initiating arcing with the consumable electrode. High-purity argon gas was used at 150–200 L/min to create an inert atmosphere. Once a steady state was achieved, melting parameters were recorded every minute and systematically logged in Table 8.

TABLE 7 – Compositions of the original (ANF-6 slag) and experimental (Model slag) slags

Slag	CaF_2	Al_2O_3	CaO	MgO	SiO_2	FeO	P	S
Original	$70 \pm 1\%$	$30 \pm 1\%$	$\leq 0.3\%$	$\leq 0.3\%$	$\leq 0.3\%$	$\leq 0.3\%$	$\leq 0.0005\%$	$\leq 0.03\%$
Model	$43 \pm 1\%$	$32 \pm 1\%$	$15 \pm 1\%$	$4 \pm 1\%$	$5 \pm 1\%$	$\leq 0.3\%$	$\leq 0.0005\%$	$\leq 0.03\%$

TABLE 8 – Parameters for the electroslag remelting process

Parameter	Value
Mold height/mm	3000
Mold diameter/mm	800
Slag mass/kg	150
Ar flow rate/($\text{L}\cdot\text{min}^{-1}$)	150–200
Secondary voltage/V	42–52
Alternating current/A	10000–13000
Average melting rate/($\text{kg}\cdot\text{min}^{-1}$)	10.0–10.5

3.2 Industrial experimental results

Figure 3 illustrates a smooth surface of the ESR ingot with an easily detachable thin slag skin during deslagging. This observation indicates that the physical properties of the model slag, such as melting point and viscosity, are well-suited for electroslag remelting, confirming its superior processability.



FIG 3 – The ESR ingot remelted by model slag

After forging and heat treatment, samples with dimensions of 10 mm × 20 mm × 20 mm was cut from the axial center of the slab with 180 mm × 1200 mm cross section, used for inclusion detection. Figure 4 shows the calcium content of the electrode and ESR ingot, along with the inclusion rating results. Regarding inclusion rating, a notable reduction in the number and size of D/Ds inclusions was observed after adopting the model slag. In terms of elemental content, it was noted that the calcium concentration in ESR ingots significantly decreased with the introduction of the Model slag.

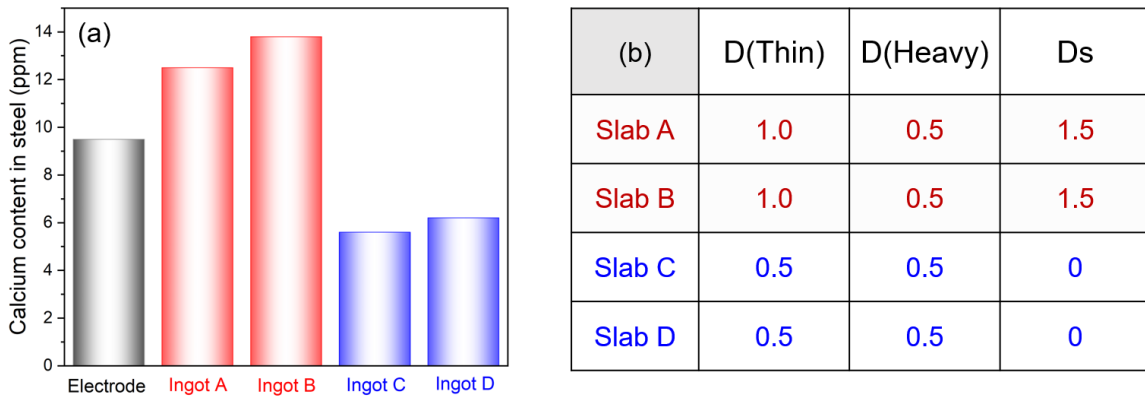


FIG 4 – (a) Calcium content in electrode and ingots; (b) D and Ds inclusion rating results. Ingots A and B (Slabs A and B) were smelted using ANF-6 slag, while ingots C and D (Slabs C and D) were smelted using the model slag.

Data from Figure 4(a) indicates that, passing through the ANF-6 slag pool, the calcium content in Ingot A and Ingot B shows an increase trend relative to the raw consuming electrode. Conversely, when metal droplets traverse the Model slag pool to form Ingot C and Ingot D, there is a noticeable decrease in calcium content compared to the electrode. Given that calcium is not a required element in electrode alloys and primarily exists in the form of inclusions in the electrode, the reduction of calcium content during electroslag remelting is not attributable to the loss of dissociative calcium elements in the electrode matrix. This phenomenon suggests that the Model slag pool could effectively reduce the calcium content in the ingots by absorbing calcium-containing inclusions in the electrode. This is consistent with the results in Figure 5, which depicts electron microscopy scans of typical D and Ds inclusions in ESR ingots remelted using ANF-6 slag and Model slag. The results show a reduction in inclusion size and dramatically decreased concentrations of Ca in ingots remelted with the Model slag.

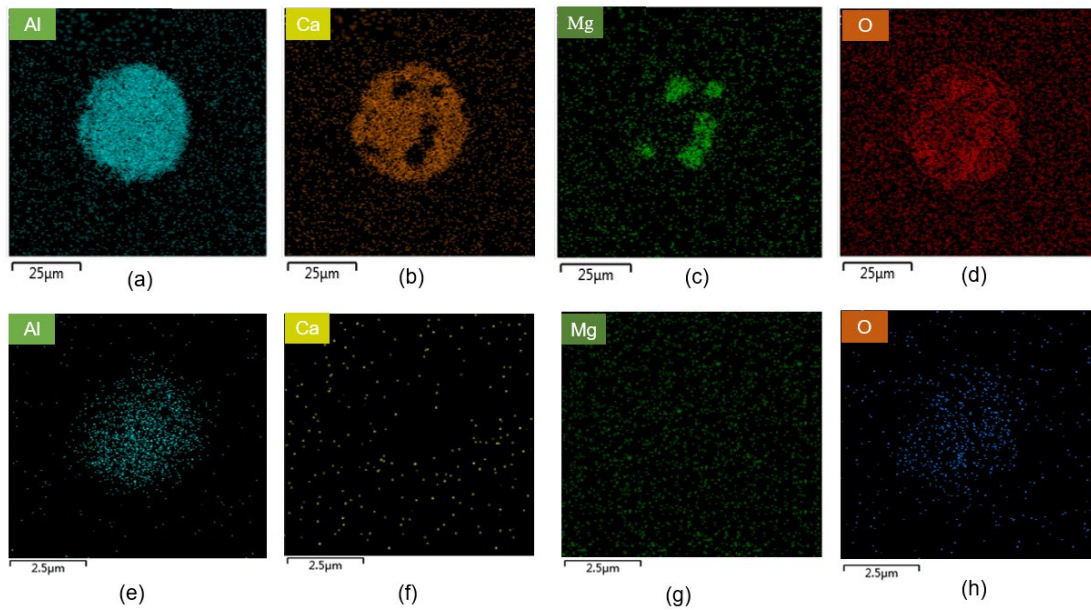


FIG 5 – (a), (b), (c), (d) SEM images of inclusions in Slab A remelted using ANF-6 slag; (e), (f), (g), (h) SEM images of inclusions in Slab C remelted using the model slag

The industrial experimental results demonstrated that the utilization of the Model slag not only preserved the excellent surface quality of the ingots but also effectively removed the excessive D and Ds inclusions in 1.2343 die steel.

3.3 Discussion

Based on MICT theory, the free calcium ions concentrations in ANF-6 slag and Model slag have been calculated. The results reveal a positive correlation between free calcium ion concentrations in molten slag and calcium content in ingots, as depicted in Figure 6. When remelting the steel with ANF-6 slag, due to sufficient slag-metal reaction, high free calcium ions in molten slag could lead to “calcium treatment” on the original Al_2O_3 type inclusion in electrode. Thus, higher calcium content and excessive $\text{CaO-Al}_2\text{O}_3$ (D and Ds inclusions) have been detected in the slab. While, remelted with the Model slag with low free calcium ions concentration, the “calcium treatment” effect have been effectively suppressed. Furthermore, calcium ions in liquid steel could diffuse into the molten slag driven by the concentration gradient. This could explain well that fewer calcium content and less D and Ds inclusions have been detected in the 1.2343 steel remelted with model slag.

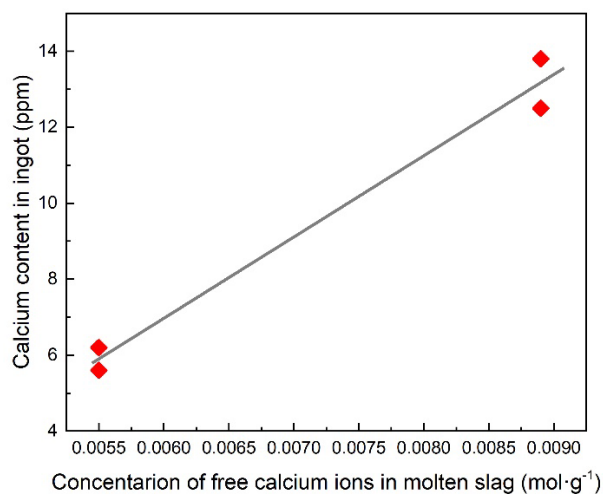


FIG 6 – Correlation between free calcium ion concentration in the slag and calcium content in the ESR ingot

This work has utilized the molecule ion coexistence theory to calculate the effects of varying mass percentages of CaF_2 , Al_2O_3 , CaO , SiO_2 , and MgO on the activity of calcium ions at 1550°C . Mass percentages of these components will range from 30% to 70% for CaF_2 , 20% to 40% for Al_2O_3 , 0% to 40% for CaO , 0% to 15% for SiO_2 , and 0% to 15% for MgO , with each component varying in 1% increments across all possible combinations. The calculated results presented in Figure 7(a) reveal that the correlation coefficient for CaF_2 is the highest, indicating that the concentration of CaF_2 in the slag directly affects the concentration of free calcium ions in the molten state. Furthermore, with the mass fraction of CaF_2 held constant, the impact of other components on the concentration of free calcium ions was calculated, shown in Figure 7(b).

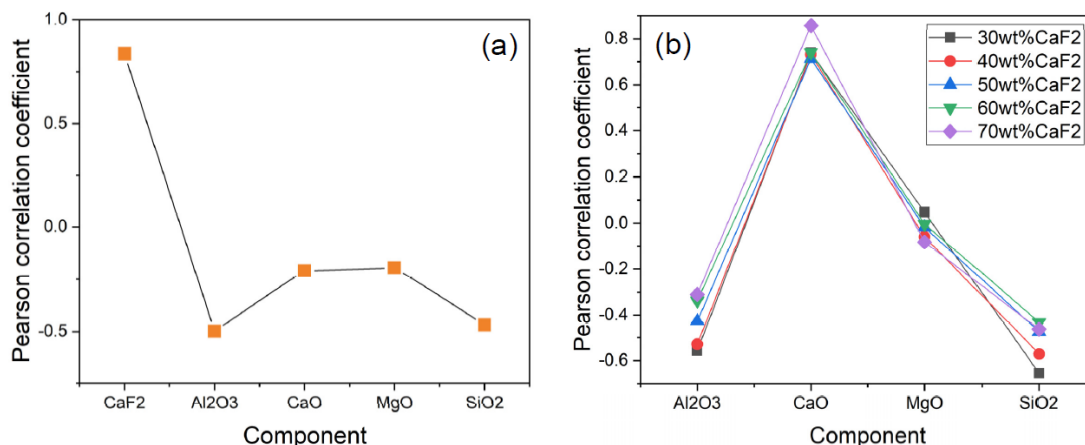


FIG 7 – Correlation coefficient for the relationship between each component and calcium ion concentration based on the molecule–ion coexistence theory: (a) Pearson correlation coefficients of each component with free calcium ion concentration; (b) Influence of other components on free calcium ion concentration when the CaF_2 mass fraction is fixed

The Pearson correlation coefficients in Figure 7 show that CaF_2 significantly affects the concentration of free calcium ions in the slag. Additionally, the concentration of CaO also exerts an influence. Conversely, the concentration of MgO in the slag system has minimal impact on the concentration of free calcium ions. Moreover, Al_2O_3 and SiO_2 in the slag system moderately suppress the concentration of free calcium ions.

4. CONCLUSION

1. Employing well-defined screening criteria, the slag composition exhibiting superior performance was theoretically selected. Subsequent experimental verification confirmed the exceptional performance of this new slag composition, thereby demonstrating the feasibility and efficiency of using genetic algorithms for slag system optimization.
2. CaF_2 and CaO were identified to increase the activity of calcium ions in the slag, with CaF_2 exerting a greater effect than CaO . SiO_2 and Al_2O_3 were observed to decrease calcium ion activity, with SiO_2 being slightly more effective than Al_2O_3 in this aspect. Meanwhile, MgO demonstrated no significant impact on calcium ion activity.
3. To further reduce the concentration of free calcium ions and free alumina activity in the slag, it is recommended to decrease the content of CaF_2 and increase the contents of CaO and SiO_2 .

ACKNOWLEDGEMENTS

This work was supported by Program of Introducing Talents of Discipline to Universities (No.B21001), Science and Technology Research Projects of Liaoning Province (2023JH1/10400051).

REFERENCES

- Birol, B, Polat, G and Saridede, M N, 2015. Estimation Model for Electrical Conductivity of Molten CaF_2 - Al_2O_3 - CaO Slags Based on Optical Basicity, *JOM*, 67: 427-435.

- Campbell, C and Olson, G, 2000. Systems design of high performance stainless steels I. Conceptual and computational design, *Journal of Computer-Aided Materials Design*, 7: 145-170.
- Dong, Y W, 2007. Mathematical Modeling of Solidification during Electroslag Remelting Process and Development of New Slags, PhD thesis, Northeastern University, Shenyang.
- Dong, Y W, Jang, Z H and Yu, A, 2016. Dissolution Behavior of Alumina-Based Inclusions in $\text{CaF}_2\text{-Al}_2\text{O}_3\text{-CaO-MgO-SiO}_2$ Slag Used for the Electroslag Metallurgy Process, *METALS*, 6: 272-279.
- Dong, Y W, Jiang, Z H, Cao, Y L, Yu, A. and Hou, D, 2014. Effect of Slag on Inclusions During Electroslag Remelting Process of Die Steel, *Metallurgical and Materials Transactions B*, 45: 1315-1324.
- Duan, S C, 2020. Fundamental Study on the Controlling Loss of Alloying Elements of Large IN718 Electroslag Remelting Ingots, PhD thesis, University of Science and Technology, Beijing.
- Duchesne, M A and Hughes, R W, 2017. Slag density and surface tension measurements by the constrained sessile drop method, *Fuel*, 188: 173-181.
- Guillot, B and Guissani, Y, 1996. Towards a theory of coexistence and criticality in real molten salts, *Molecular Physics*, 87: 37-86.
- Guo, Y, Xia, Z, Shen, Z, Li, Q, Sun, C, Zheng, T and Ren, W, 2021. Enhancement of removing inclusions from liquid melt film during the ESR process assisted by a static magnetic field, *Journal of Materials Processing Technology*, 290: 1-9.
- Hao, X and Wang, X H, 2016. A New Sulfide Capacity Model for $\text{CaO-Al}_2\text{O}_3\text{-SiO}_2\text{-MgO}$ Slags Based on Corrected Optical Basicity, *Steel Research International*, 87: 359-363.
- Jang, W F, Tian, L, Bo, H and Ma, T F, 2023. A new method for evaluating the melting performance of the slag, *Ironmaking & Steelmaking*, 50: 775-781.
- Jang, Z H, Dong, Y W, Geng, X and Liu, F B, 2015. *Physical Chemistry and Transport Phenomena During Electroslag Metallurgy* pp 68-75 (Northeastern University Press: Shenyang).
- Jiang, Z H, Dong, Y W, Geng, X and Liu, F B, 2023. Development and application of electroslag remelting technology for high quality special steels, *Iron & Steel*, 58: 15-25.
- Ju, J T, Gu, Y and Zhang, Q, 2021. Effect of CaF_2 and $\text{CaO/Al}_2\text{O}_3$ ratio on evaporation and melting characteristics of low-fluoride $\text{CaF}_2\text{-CaO-Al}_2\text{O}_3\text{-MgO-TiO}_2$ slag for electroslag remelting, *Ironmaking & Steelmaking*, 50: 8.
- Ju, J, Ji, G, Tang, C, Yang, K and Zhu, Z, 2020. Investigation of fluoride evaporation from $\text{CaF}_2\text{-CaO-Al}_2\text{O}_3\text{-MgO-TiO}_2\text{-(Li}_2\text{O)}$ slag for electroslag remelting, *Scientific Reports*, 10: 1-12.
- Ju, J, Lv, Z L and Jiao, Z Y, 2012. Experimental Study on the Electrical Conductivity of $\text{CaF}_2\text{-SiO}_2\text{-Al}_2\text{O}_3\text{-CaO-MgO}$ Slag System, *Journal of Iron and Steel Research International*, 24: 27-31.
- Li, J X and Zhang, J, 2000. $\text{CaO-MgO-CaF}_2\text{-Al}_2\text{O}_3\text{-SiO}_2$ Five-element slag system Calculation model of viscosity, *Journal of University of Science and Technology Beijing*, 22: 316-319.
- Liu, J H, Zhang, G H, Wu, Y D and Chou, K C, 2016. Study on electrical conductivity of $\text{Fe}_x\text{O-CaOSiO}_2\text{-Al}_2\text{O}_3$ slags, *Canadian Metallurgical Quarterly*, 55: 221-225.
- Ragnarsson, L and Sichen, D, 2009. Inclusions Generated during Ingot Casting of Tool Steel, *steel Research International*, 81: 40-47.
- Sabih, A, Wanjara, P and Nemes, J, 2005. Characterization of internal voids and cracks in cold heading of dual phase steel, *ISIJ International*, 45: 1179-1186.
- Schneider, R S E, Molnar, M, Kloesch, G and Schueller, C, 2019. Effect of the Al_2O_3 Content in the Slag on the Chemical Reactions and Nonmetallic Inclusions during Electroslag Remelting, *Metallurgical and Materials Transactions B*, 51: 1904-1911.
- Sebastian, R and Bernd, F, 2015. Influencing the Electroslag Remelting Process by varying Fluorine Content of the utilized Slag. *The 8th European Metallurgical Conference (EMC)*. Düsseldorf.
- Sebastian, R and Bernd, F, 2015. Process and Refining Characteristics of ESR using MgO containing Slag Systems. *International Symposium on Liquid Metal Processing & Casting*. Leoben/Germany.
- Sebastian, R, Johannes, M and Bernd, F, 2012. The Influence of Selected Slag Properties and Process Variables on the Solidification Structure during ESR. *1st International Conference on Ingot Casting, Rolling and Forging (ICRF)*. Aachen/Germany.
- Shi, C B, Li, J, Cho, J W, Jiang, F and Jung, I H, 2015. Effect of SiO_2 on the Crystallization Behaviors and In-Mold Performance of $\text{CaF}_2\text{-CaO-Al}_2\text{O}_3$ Slags for Drawing-Ingot-Type Electroslag Remelting, *Metallurgical and Materials Transactions B*, 46(B): 2110-2120.
- Shi, C, 2020. Deoxidation of Electroslag Remelting (ESR) – A Review, *ISIJ International*, 60: 1083-1096.

- Sun, H, Yang, J, Zhang, R H and Yang, W K, 2021. Effect of Slag Basicity on Dephosphorization at Lower Basicity and Lower Temperature Based on Industrial Experiments and Ion-Molecular Coexistence Theory, *Metallurgical and Materials Transactions B*, 52: 3403-3422.
- Wan, X X, Shi, C B, Yu, Z and Li, J, 2022. Effect of CaF_2 and Li_2O on structure and viscosity of low-fluoride slag for electrosag remelting of rotor steel, *Journal of Non-Crystalline Solids* 597: 121914.
- Xu, W, Delcastillo, P E J R D and Van Der Zwaag, S, 2009. A combined optimization of alloy composition and aging temperature in designing new UHS precipitation hardenable stainless steels, *Computational Materials Science*, 45: 467-473.
- Yi, H, Shi, C B, Wan, X X, Liang, Y J, Li, J and Liu, S J, 2022. Viscosity and surface tension of CaF_2 - CaO - Al_2O_3 -based slag with varying SiO_2 and B_2O_3 contents for ESR of rotor steel, *Journal of Iron and Steel Research International*, 30: 74-81.
- Zhang, G H, Chou, K C and Pal, U, 2013. Estimation of Sulfide Capacities of Multicomponent Slags using Optical Basicity, *ISIJ International*, 53: 761-767.
- Zhao, M G, Li, G and He, S P, 2022. Study of Thermodynamic for Low-Reactive CaO - BaO - Al_2O_3 - SiO_2 - CaF_2 - Li_2O Mold Flux Based on the Model of Ion and Molecular Coexistence Theory, *Metals*, 12: 1099
- Zhao, X H, Zhang, Z H and Ju, J T, 2013. Study on Melting Temperature of CaF_2 - SiO_2 - Al_2O_3 - CaO - MgO Slag, *Hot Working Technology*, 42: 81-84.